JOURNAL OF GUIDANCE, CONTROL, AND DYNAMICS
Vol. 32, No. 6, November–December 2009

Practical Steering Law for Small Satellite Energy Storage and Attitude Control

David J. Richie* and Vaios J. Lappas†
University of Surrey, Guildford, England GU2 7XH, United Kingdom
and
Bong Wie‡
Iowa State University, Ames, Iowa 50011-2271

DOI: 10.2514/1.41968

Recent practical work in developing combined energy storage and attitude control subsystems for small satellites has opened the door to more complex, demanding space missions. Laden with substantial benefits, these efforts use variable-speed control moment gyroscopes to store and drain energy while controlling satellite orientation. The full nonlinear equations for simultaneous control of gimbal and wheel motors for this system were theoretically unraveled in previous work but assumed that a single computer dictates the commands to these motors at each time step. This method renders it impossible to control the wheel and gimbal motors separately: a requirement for immediate flywheel implementation in contemporary satellite energy storage subsystems. Such isolated flywheel control would impart disturbance torques from torquing the wheel motors through passive electronic circuits. This torque then must be accommodated by the gimbal steering law, which is also tasked with slewing the satellite. To address this need, a novel gimbal steering law is derived to permit independent gimbal and wheel control of the actuators with continued singularity avoidance: a situation that allows direct incorporation of such a system into an existing small satellite energy storage subsystem.

Nomenclature

$D^\sharp$	=	suitable pseudoinverse logic for matrix D
e	=	variable-limiter proportional-plus-integral-plus-derivative integral error matrix
G	=	generalized singularity robust dither matrix
H_x, H_y, H_z	=	control-moment-gyroscope angular momentum in three dimensions, N · m · s
h	=	angular momentum, N · m · s
Iw_{s_d}	=	diagonal gyro wheel spin-axis inertia matrix, kg · m^2
$I_{G_j}, I_{W_j}, I_{\text{sc}}$	=	gimbal, wheel, and satellite bus inertia matrices, kg · m^2
n	=	number of cluster actuators
P_e	=	power tracking error, W
$q(\beta)$	=	matrix function of attitude quaternion β
V	=	wheel spin-axis momentum matrix
β_e	=	largest quaternion error (measured at each time step)
θ	=	control-moment-gyroscope pyramid angle, deg
κ	=	control-moment-gyroscope singularity index
μ, μ_2	=	variable-speed control-moment-gyroscope pseudoinverse singularity avoidance exponent
$\bar{\Omega}, \dot{\bar{\Omega}}$	=	estimated wheel speed, wheel acceleration
$\dot{\Omega}$	=	maximum wheel acceleration, rad/s^2
Ω_j	=	j_{th} wheel speed, rad/s

Subscripts

a	=	actual
c	=	command, commanded
d	=	disturbance (e.g., attitude torque)
g	=	control-moment-gyro gimbal axis
i	=	i_{th} object (e.g., $i = 1, 2, 3, 4$ or $i = 1, 2, 3$)
j	=	j_{th} object (e.g., $j = 1, 2, 3, 4$ or $j = 1, 2, 3$)
m	=	measured value (e.g., attitude orientation, rate)
r	=	reference or required
s	=	control-moment-gyro spin axis
sc	=	spacecraft (satellite)
t	=	control-moment-gyro transverse axis
w, wh	=	wheel (rotor, shaft, and motor)
(0)	=	initial condition value (e.g., initial wheel speed)
1, 2a, 2b	=	steering-law identifiers

I. Introduction

BECAUSE OF advancing technology and miniaturization, today's small satellites (less than 500 kg) are increasingly used for more complex missions. One method that enables this complexity increase at reduced mass is combining subsystems. Combined energy storage and attitude control subsystems (ESACS) achieve this need through consolidating actuator components. Specifically, flywheel-based momentum-exchange devices can be used not only in traditional satellite pointing control roles but also as dynamos to store primary source energy (e.g., from solar arrays) then drain it, passing secondary power to the satellite's subsystems during eclipse. This assumes that minimal energy is maintained in these flywheel batteries such that these actuators can provide adequate pointing control while serving as dynamos. Three basic momentum-exchange actuator approaches can satisfy this ESACS concept: counter-rotating flywheels, redundant flywheel clusters (e.g., at a minimum for three-axis control this implies at least four wheels in a tetrahedron), and variable-speed control moment gyroscopes (VSCMGs). The term ESACS is used here instead of the older integrated power and attitude control subsystem (IPACS), as an IPACS implies that simultaneous (i.e., integrated) command solutions are sent to the attitude and power

Presented as Paper 7501 at the AIAA/AAS Astrodynamics Specialist Conference and Exhibit, Honolulu, HI, 18–21 August 2008; received 3 November 2008; revision received 20 June 2009; accepted for publication 29 June 2009.

*Major, U.S. Air Force; Ph.D. Graduate, Surrey Space Centre, School of Electronics and Physical Sciences; d_j_richie@yahoo.com. Senior Member AIAA.

†Senior Lecturer, Surrey Space Centre, School of Electronics and Physical Sciences; v.lappas@surrey.ac.uk. Member AIAA.

‡Professor, Department of Aerospace Engineering; bong.wie@iastate.edu. Associate Fellow AIAA.

actuators, whereas the more generic ESACS term includes the IPACS versions as well as independent steering implementations (e.g., the decoupled and one-way coupled steering cases shown later). Also note that CMGs and VSCMGs are typically single- or double-gimbaled flywheels (more than two gimbals for each CMG actuator does not add value, whereas double-gimbal CMGs have better singularity avoidance properties but are less efficient than the single-gimbal variety). For the purpose of this work, the term VSCMG is used to connote single-gimbal CMGs with variable-speed flywheels. Because VSCMGs combine torque-amplification advantages of CMGs (an efficiency improvement over momentum wheels) with variable-speed flywheels for singularity avoidance and power tracking, the VSCMG is assumed to be the best actuator for an ESACS[§].

As well summarized in [2,3], this technology has a rich literary background for both satellite flywheel energy storage and CMGs dating back to 1961 ([4,5], respectively). Key highlights (from well over 600 works) include magnetic bearing and composite rotor technology advancements in [6–13] CMG/VSCMG nonlinear equations of motion and singularity avoidance in [5,14–20], counter-rotating flywheels in [21–28], and VSCMG-based ESACS in [29–31]. More recently, the work in [32–35] combined efforts in small satellite CMG sizing/technology demonstration, small satellite ESACS sizing using counter-rotating flywheels, and the VSCMG-based ESACS theory mentioned previously to identify key benefits: namely agile-slewing, high peak-power density with moderate energy density, and long lifetime (i.e., through magnetic bearings). Despite extensive research over 48 years, none of the references identified here addressed the practical case of independent wheel motor and gimbal motor control to meet the desired attitude and power profiles.

A generic simultaneous ESACS closed-loop block diagram is captured in Fig. 1. As one can see, a reference attitude profile and a reference power storage profile are met through the use of a common actuator set (in this case, a VSCMG cluster). The actuators convert the reference power profile and attitude command torque (from a vehicle control law) into wheel motor and gimbal motor commands. The motors then convert the command inputs into physical motion. This physical motion (i.e., wheel and gimbal state changes) forms the physically applied actuator torque and power to the satellite. The applied actuator torque plus disturbance torques then drive the satellite dynamics, which results in motion measured by the attitude sensors. These sensors feed these data back for input into the attitude controller. The power system is assumed to operate in an open-loop mode for this model. This process is then iterated.

The key idea illustrated in Fig. 1 is that for the simultaneous VSCMG-based ESACS, the wheel and gimbal motors are commanded (i.e., $\dot{\Omega}_c, \dot{\delta}_c$) through a consolidated steering law (as shown in [30,36,37]). However, in the practical case, $\dot{\Omega}_c$ represents the wheel motor commands implemented via a passive electrical circuit, which is solely driven by the needs of the energy storage subsystem (i.e., through P_r). This means that $\dot{\delta}_c$ not only must be used to modify the satellite attitude, but also must accommodate torques generated by the cluster from the independent control of $\dot{\Omega}_c$. The difference of these two approaches will be compared in this paper.

[§]Use of the terms *flywheel*, *momentum wheel*, and *reaction wheel* in the literature is not uniform, depending upon how these terms are defined [1]. This paper employs the definitions for these terms from [1]: A flywheel "is any rotating wheel or disk used to store or transfer momentum," a momentum wheel "is a flywheel designed to operate at a biased, or nonzero, momentum" that "provides a variable-momentum storage capability about its rotation axis, which is usually fixed in the vehicle," and a reaction wheel "is a flywheel with a vehicle-fixed axis designed to operate at zero bias." Note that, "the same momentum can be achieved with a small, high-speed flywheel as with a large low-speed one" [1]. If the flywheel sizes are equal, then a reaction wheel has to change through a larger speed range than a momentum wheel to impart the same torque, because of its zero bias. Using the preceding definitions, because both reaction wheels and momentum wheels each use a fixed-axis flywheel with speed change capability to produce disturbance rejection and slewing torques, the term *variable-speed flywheel mode* (or simply *wheel mode*) is used throughout the paper to convey a fixed-axis flywheel (or set of flywheels) that changes (change) speeds to impart control torque as opposed to the fixed-speed, gimbaled flywheel mode of a CMG.

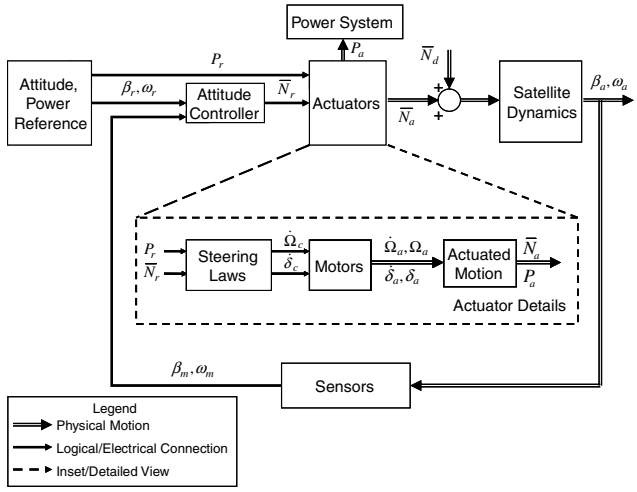

Fig. 1 Attitude control block diagram with CMG steering architecture inset.

In short, this work fills a practical gap in the existing literature through examining the impact of separating the wheel motor from the gimbal motor functions as it compares with the simultaneous steering case. However, this work also goes a step further through analyzing the impact that oversimplification of the problem can have when completely decoupling these two functions (as a prudent attitude control designer would be prone to do), resulting in loss of accurate pointing for significant time periods. To achieve this aim, the paper's organized into a description of the key combined attitude and power tracking mathematical model, relevant vehicle torque control laws (i.e., for stable command torque $\bar{N}_r$) typically driven by stability criteria but that can also include steady-state error performance and saturation constraints, the simultaneous attitude/power steering model developed in past work (e.g., see [30]), the practical case (both one-way coupled and completely decoupled) steering laws, numerical examples (for all three steering laws: the basic simultaneous case plus the two practical cases), discussion of results, and a summary of the paper's key contributions.

II. Combined Attitude and Power Tracking Mathematical Model

Similar to that shown in [30,38] and assuming that the desired inertial attitude state is not angularly accelerating and the system total inertia remains constant over the given maneuver, a model encompassing the spacecraft dynamics, kinematics, required attitude reference torque, and VSCMG attitude steering is

$$\dot{\beta} = \tfrac{1}{2} q(\beta)\omega \tag{1}$$

$$q(\beta) = \begin{bmatrix} -\beta_1 & -\beta_2 & -\beta_3 \\ \beta_0 & -\beta_3 & \beta_2 \\ \beta_3 & \beta_0 & -\beta_1 \\ -\beta_2 & \beta_1 & \beta_0 \end{bmatrix} \tag{2}$$

$$\bar{N}_d = I_T\dot{\omega} + \tilde{\omega} I_T\omega + B\ddot{\delta} + E\dot{\Omega} + D\dot{\delta} + F\Omega \tag{3}$$

$$\bar{N}_r = -I_T\dot{\omega} - \tilde{\omega} I_T\omega \tag{4}$$

$$I_T\dot{\omega} = -K(\omega - \omega_r) + kq^T(\beta)\beta_r \tag{5}$$

$$\bar{N}_r = K(\omega - \omega_r) - kq^T(\beta)\beta_r - \tilde{\omega} I_T\omega \tag{6}$$

$$\bar{N}_r + \bar{N}_d = B\ddot{\delta} + E\dot{\Omega} + D\dot{\delta} + F\Omega \tag{7}$$

where $\bar{N}_d$ is the inertial torque acting on the combined system of the spacecraft platform plus the VSCMGs; I_T is the system inertia, assuming that the gimbaled VSCMG inertia (from rotor dynamics) is negligible; β is the Euler parameter set (β_0, β_1, β_2, β_3) representing the satellite body-frame orientation with respect to the inertial frame, ω is the angular velocity of the body frame with respect to the inertial frame expressed in body-frame coordinates; $\dot{\beta}$ and $\dot{\omega}$ are the body-frame time derivatives of β and ω; β_r and ω_r are command reference versions of β and ω; δ is an $n \times 1$ column matrix of n-VSCMG gimbal angles; $\dot{\delta}$ and $\ddot{\delta}$ are $n \times 1$ gimbal angular velocity and angular acceleration column matrices; $\tilde{\omega}$ is a 3×3 skew-symmetric matrix using the elements of ω; B, D, E, and F are $3 \times n$ matrices transforming actuator parameters from the gimbal coordinate frame to the body frame (where B is a function of δ and is constant in the body frame; D depends on ω, δ, and Ω, varies in the body frame, and is approximated as its wheel angular momenta component; E transfers the wheel acceleration to the body frame and is dependent upon the gimbal angles; and F depends on the gimbal angles and body angular velocity ω); $F\Omega$ is equivalent to the $\tilde{\omega}h$ defined in [37,39]; k is a positive gain scalar; and K is a 3×3 positive definite gain matrix. Equation (5) is a rearrangement of the stable tracking condition

$$K(\omega - \omega_r) = -I_T\dot{\omega} + kq^T(\beta)\beta_r$$

from [30], having applied the assumptions that $\dot{I}_T(\omega - \omega_r)$ and $\dot{\omega}_r$ are both 3×1 matrices of zeros. Thus, $\bar{N}_r$, which uses k and K, is the required torque for stable spacecraft attitude tracking.

Noted often in the literature (e.g., [30,40]), CMGs typically exploit torque-amplification properties through gimbal rate control (i.e., keeping gimbal motor torques small such that $\ddot{\delta} \approx 0$). The result is a velocity-based steering law to replace Eq. (7) (assuming that no external torques are applied):

$$E\dot{\Omega} + D\dot{\delta} = \bar{N}_r - F\Omega \tag{8}$$

This velocity-based steering law permits different combinations of gimbal rate and wheel acceleration (similarly torque) to achieve a desired attitude maneuver.

A. Singularity Problem

A large advantage to using CMGs in a satellite attitude control subsystem (ACS) comes from the torque-amplification property best described in [41], in which the output torque for a CMG is much larger than its input gimbal motor torque for an equivalent reaction- or momentum-wheel design, as the CMG takes advantage of fixed wheel speed momentum in generating such torque. However, a primary limitation of CMG clusters is that there are certain configurations of a CMG cluster (assuming that these CMGs use a single-gimbal design approach) in which the commanded torque from the vehicle control law cannot be produced in at least one direction. These configurations are known as singularity states and have been well studied in the existing literature. However, the variable-speed capability of VSCMGs, on the other hand, helps neutralize this effect. This is best seen in comparing the well-known CMG saturation singularity surface (left plot of Fig. 2) with the VSCMG saturation singularity surface (right plot of Fig. 2). Note that the singular regions (voids) of the CMG momentum envelope are filled in the case of VSCMGs because the VSCMGs change mode to use variable-speed flywheel mode near singularity.

B. Flywheel Energy Storage

Flywheel battery operating principles follow from the previous work addressed in [42] and tie the kinetic energy of flywheels to the power stored in and drained from these wheels. For n actuators, the total energy is just the sum of each of the individual actuator energies:

$$T_W = \sum_{j=1}^{n} \frac{1}{2} I_{W_j} \Omega_j^2 \tag{9}$$

Taking the first derivative of the energy yields the power generated in the wheels. Recall that P_r is the required power to store/drain in the wheels, and P_w is the actual power contained in the wheels. Because $V = \Omega^T I w s_d$, then $P_w = V\dot{\Omega}$, and thus

$$P_w = V\dot{\Omega} = \Omega^T I_{W_{sd}} \dot{\Omega} \tag{10}$$

Now note that P_w for this dynamic Eq. (10) is equivalent to the actuated power for the sized system, P_a, when the wheel speed Ω and wheel acceleration $\dot{\Omega}$ are at maximum values. Also note that the P_r used in sizing the system is merely the maximum allowable $P_r(t)$ per these dynamic flywheel equations.

III. Vehicle Controllers

There are two main vehicle attitude controllers that are relevant to the given problem. The first of these is the Lyapunov controller presented in [30,31,42], which involves driving the inertial angular

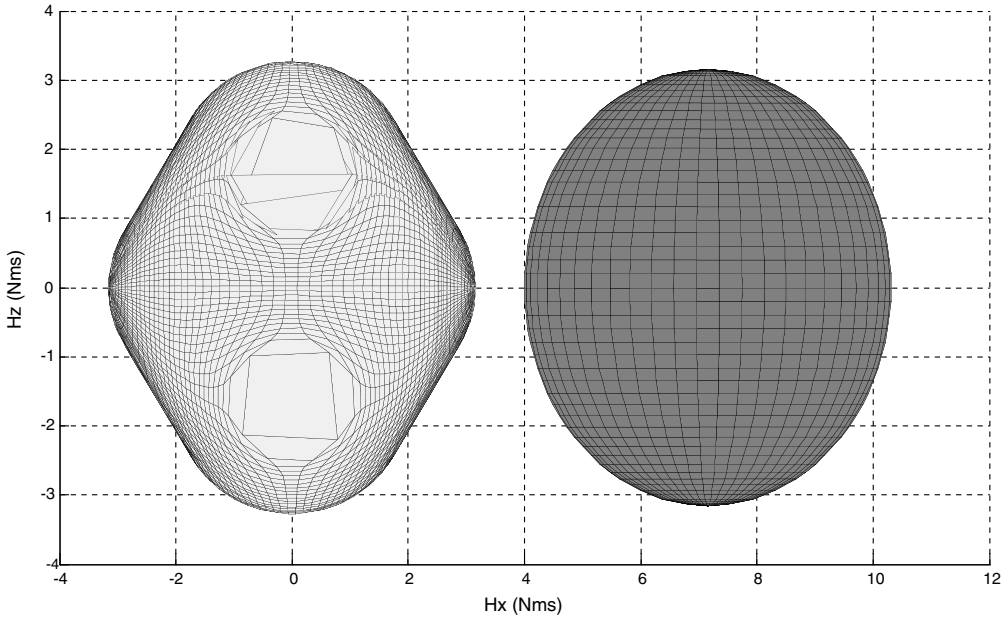

Fig. 2 Pyramid cluster CMG and VSCMG momentum envelopes.

position and angular velocity errors to zero based on attitude and power tracking requirements. The second controller, known as the variable-limiter proportional-plus-integral-plus-derivative (VLPID) controller presented by Wie et al. [19] and Heiberg et al. [43], adds terms to the Lyapunov controller to control steady-state performance and enforce key parameter saturation limits in addition to the stability guarantees inherent in the Lyapunov controller. In other words, the Lyapunov controller used is essentially a proportional-derivative (PD) controller and the VLPID controller contains the PD terms plus an integral term in addition to providing a framework for including torque and gimbal rate saturation limits. That is, PID for multiple-input, multiple-output, nonlinear spacecraft attitude systems (i.e., in Euler's moment equations) is really a misnomer in the linear systems sense, but appropriate because the gains multiply position, velocity, and position integral errors. The VLPID and Lyapunov controllers in terms of enforcing asymptotic stability are the same. Essentially, the VLPID is more general than the Lyapunov controller. However, the VLPID (as shown in [19,43,44]) helps account for torque and gimbal rate saturation and permits adding some desired steady-state performance to the stable tracking of the nonlinear-PID/Lyapunov controller described. Note that both of these controllers were applied to several numerical examples (including all three shown later), but the VLPID performance exceeded the Lyapunov performance in each case. Because of its generality, benefits, and demonstrated performance, the VLPID controller is the preferred vehicle controller of choice. Regardless, it is instructive to mathematically summarize each of these controllers next.

A. Lyapunov

The equation for an applicable Lyapunov controller is

$$\bar{N}_r = K(\omega - \omega_r) - kq^T(\beta)\beta_r - \tilde{\omega} I_T \omega \tag{11}$$

Note that the key information of this controller is the current vehicle angular position and angular velocity. As shown in [30,31,38,42], this controller stably tracks the desired attitude position and attitude rates of the system. Although developed from a Lyapunov-based stability analysis approach, this controller is also often termed a PD controller because it has a proportional gain related to the position error and a derivative (rate) gain multiplied by the rate error. However, it does lack direct accommodation of actuator and vehicle saturation limits. In contrast, these items are included in the VLPID controller, highlighted next.

B. Variable-Limiter PID

The VLPID was originally developed by Heiberg et al. [43] and further applied in [19,44]. Because of its integral term, it allows for more accurate steady-state control while driving the present vehicle position to the desired position. An added bonus, though, is the inclusion of actuator and vehicle saturation limits. This controller permits one to not only include the desired damping ratio (which affects percent overshoot) and settling time, but to also command torque limits based on actuator capabilities, momentum saturation terms (which is driven by the maximum wheel speed), gimbal rate saturation limits, and, optionally, if applying the results from [45], gimbal angle limits. Thus, not only are performance settings included along with Lyapunov-like asymptotic stability, but practical saturations limits are inherent as well. A summary of the equations governing this controller is given in Eqs. (12–16):

$$\bar{N}_r = -I_T\left(2k\,\mathrm{sat}_{L_i}\left(e + \frac{1}{T}\int e\right) + c(\omega - \omega_r)\right)T \tag{12}$$

$$L_i = \frac{c}{2k}\min(\sqrt{4a_i|e_i|}, |\omega_i|_{\max}) \tag{13}$$

$$D^{\sharp} = D^T[DD^T + \alpha G]^{-1} \tag{14}$$

$$u = -\bar{N}_r - F\Omega \tag{15}$$

$$\dot{\delta}_c = \mathrm{sat}_{\dot{\delta}_{\max}}(D^{\sharp}u) \tag{16}$$

where i varies from 1 to 3 for the general three-dimensional motion case; sat_{L_i} implies that when the term in question is saturated, it cuts off at the absolute value of L_i; $\mathrm{sat}_{\dot{\delta}_{\max}}$ saturates the term to the absolute value of $\dot{\delta}_{\max}$; a_i is the maximum permissible vehicle acceleration in the i_{th} direction; e_i is the angular position error limit; $\omega_{i_{\max}}$ is the maximum permissible vehicle velocity in the i_{th} direction; and c, k, and T are derivative, proportional, and integral inverse controller gains. The other parameters follow as before.

IV. Simultaneous Steering

As shown in [29,30,36], one can store (drain) energy by increasing (decreasing) the VSCMG wheel speeds in combinations that still permit the desired net torque for attitude tracking. The mechanics of this process are developed next. From Eqs. (8) and (10), one can define the set

$$\begin{bmatrix} E & D \\ V & 0_n \end{bmatrix} u = \begin{bmatrix} Q \\ S \end{bmatrix} u = \begin{bmatrix} N_c \\ P_c \end{bmatrix} \tag{17}$$

where $u = [\,\dot{\Omega}^T \quad \dot{\delta}^T\,]^T$, $N_c = \bar{N}_r - F\Omega$, $P_c = P_r(t)$, $Q = [\,E \quad D\,]$, O_n is a $1 \times n$ matrix of zeros, and $S = [\,V \quad 0_n\,]$. Equation (17) enables simultaneously tracking an attitude reference and a power profile, provided the rank of $[\,Q \quad S\,]^T$ is at least 4, as mentioned in [37]. From this, the fundamental VSCMG attitude steering problem is ensuring

$$Qu_c = Q\begin{bmatrix} \dot{\Omega} \\ \dot{\delta} \end{bmatrix}_c = N_c \tag{18}$$

which yields a general VSCMG steering law:

$$\begin{bmatrix} \dot{\Omega} \\ \dot{\delta} \end{bmatrix}_c = Q^{\dagger}N_c \tag{19}$$

where $Q^{\dagger}$ is some generalized inverse of Q such as

$$Q^{\dagger} = W_1Q^T(QW_1Q^T)^{-1} \tag{20}$$

in which W_1 is a weighting matrix for prioritizing the two VSCMG modes: variable-speed flywheel mode and CMG mode. As defined in [30,42,46] and others, $W_1 = [\,W_s \quad W_g\,]$, where the wheel weights are W_s and the gimbal weights are W_g.

V. Independent Steering

The physical requirements for separating the wheel and gimbal commanding stated earlier engenders a modification of the simultaneous steering equations. The simultaneous attitude and power tracking steering equation set given in Eq. (17), which follows from Eqs. (8) and (10), is composed of an attitude part (its top row) and a power part (the bottom row). The attitude part was presented as Eq. (8) and is typically used for classical, fixed rotor speed, single-gimbal CMGs. The fixed speed means that $E\dot{\Omega}$ is zero and the resulting steering law is

$$\dot{\delta}_c = D^{\dagger}(\bar{N}_r - \omega \times h) = D^{\dagger}(\bar{N}_r - F\Omega) \tag{21}$$

where $D^{\dagger}$ is the applicable pseudoinverse steering logic for several different methods, including null motion, preferred gimbal angles, singularity robust steering logic, etc., contained in the literature surveyed in [33]. Meanwhile, the energy storage part was presented in Eq. (10) and contains an individual solution of

$$\dot{\Omega}_c = V^{\dagger}P_c \tag{22}$$

Together, Eqs. (21) and (22) differ by a factor of $E\dot{\Omega}$ in the solution to Eq. (17), which seeks to find the control vector at the current time step $u_c = [\,\dot{\Omega}_c^T \quad \dot{\delta}_c^T\,]^T$ using the wheel speed measurements from the

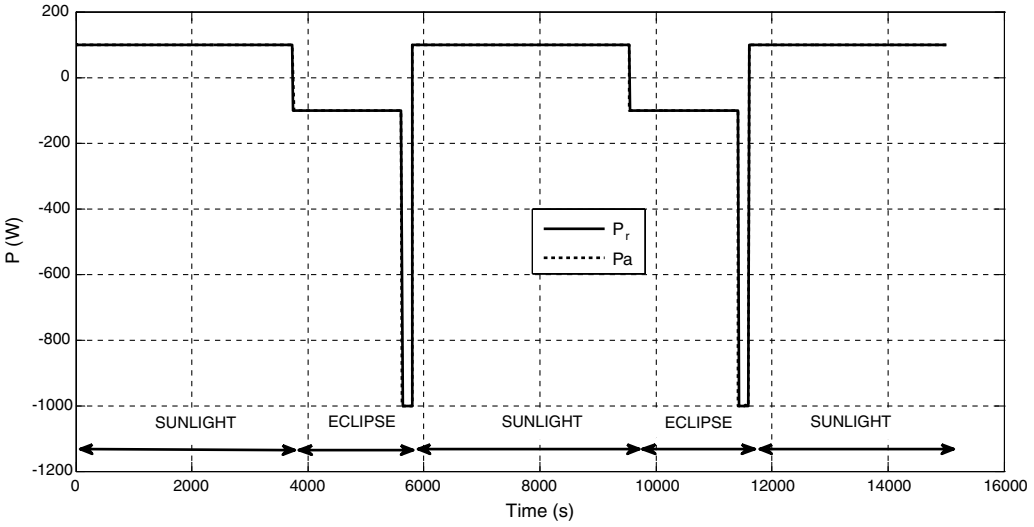

a) Power tracking

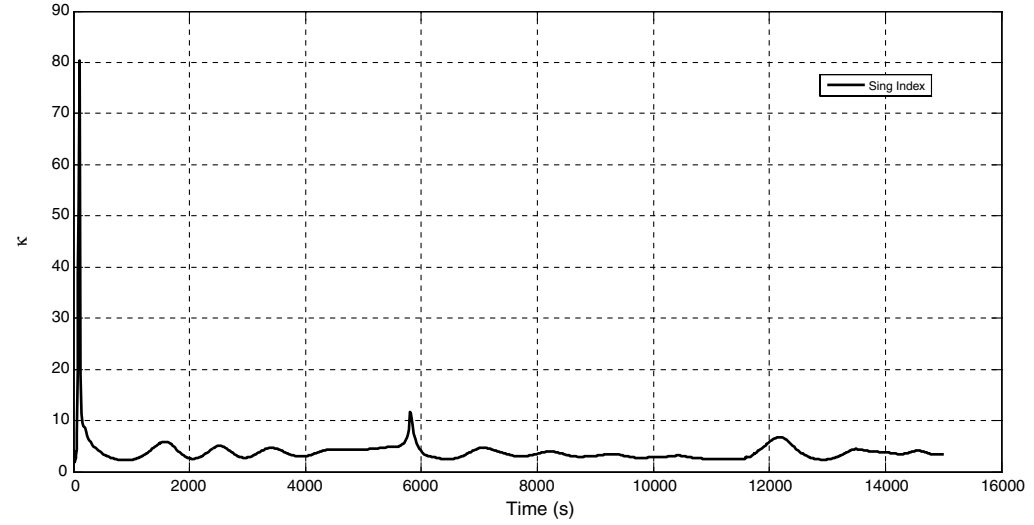

b) Singularity condition

Fig. 3 Simultaneous steering vehicle results.

previous time step Ω. In fact, Eq. (17) describes a one-way coupled system. That is, its attitude part is coupled in the control terms $\dot{\Omega}_c$ and $\dot{\delta}_c$, whereas the power equation is independent of $\dot{\delta}_c$. Thus, a practical limitation of the simultaneous steering approach is that it requires the wheel speed and gimbal rate control to be driven from the same controller with synchronized commanding of $\dot{\Omega}_c$ and $\dot{\delta}_c$. However, to be effective, the electrical power subsystem (EPS), critical to typical spacecraft, must have direct control of the battery state of charge at all times. For flywheel batteries, this means direct command of the wheel speed. Unless a paradigm shift in spacecraft EPS architecture is instantiated in which the EPS and ACS are completely integrated into one system at the initial design stage, near-term ESACS implementations will require that the EPS control $\dot{\Omega}$ through its battery charge control system. This is usually done one of two ways: via direct energy transfer (DET) or via peak-power tracking [47]. The DET control of $\dot{\Omega}$ is an integral aspect of the demonstrated ESACS in [33]. Nevertheless, from an ACS perspective, one can accommodate the loss of wheel controllability in the gimbal rate steering law by estimating the wheel acceleration in addition to the wheel velocity, provided these values are observable in the wheel motor/generator telemetry. Put another way, if the EPS is viewed as independently controlling the power part of Eq. (17), then the top part can be rearranged as

Table 1 Cases

No.	Description
1	Simultaneous steering law
2a	Decoupled steering law, $\dot{\delta}_c = D^{\dagger}(\bar{N}_r - F\bar{\Omega})$
2b	One-way coupled steering law, $\dot{\delta}_c = D^{\dagger}(\bar{N}_r - F\bar{\Omega} - E\dot{\bar{\Omega}})$

Table 2 Simulation parameters

Symbol	Value
n	4
θ, deg	54.75
$\omega(0)$, rad/s	[0 0 0]
$\beta(0)$	[−0.5 0.5 −0.5 0.5]
$\delta(0)$, rad	$[\frac{\pi}{4} - \frac{\pi}{4} - \frac{\pi}{4} \frac{\pi}{4}]$
$\dot{\delta}(0)$, rad/s	[0 0 0 0]
$\Omega(0)$, rpm	[11000 9625 8250 7150]
I_{W_j}, kg · m^2	diag{0.009946, 0.005, 0.005}
I_{G_j}, kg · m^2	diag{0.001, 0.001, 0.001}
I_{sc}, kg · m^2	$\begin{bmatrix} 120 & -5 & -3 \\ -5 & 100 & 1.5 \\ -3 & 1.5 & 100 \end{bmatrix}$
K,k	diag{0.1, 0.1, 0.1},0.01
μ,μ_2, $W_{2_{j_0}}$,$W_{g_{j_0}}$	1, 1000, 0.1, 0.1

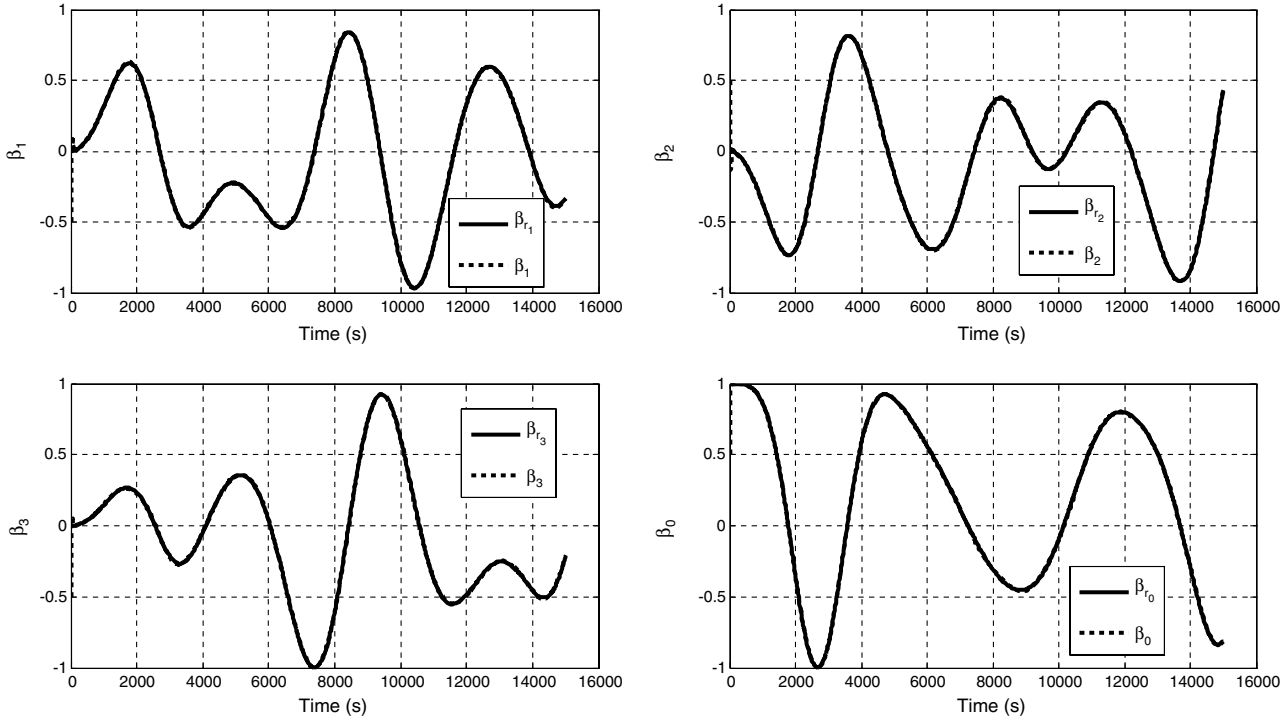

a) Angular position

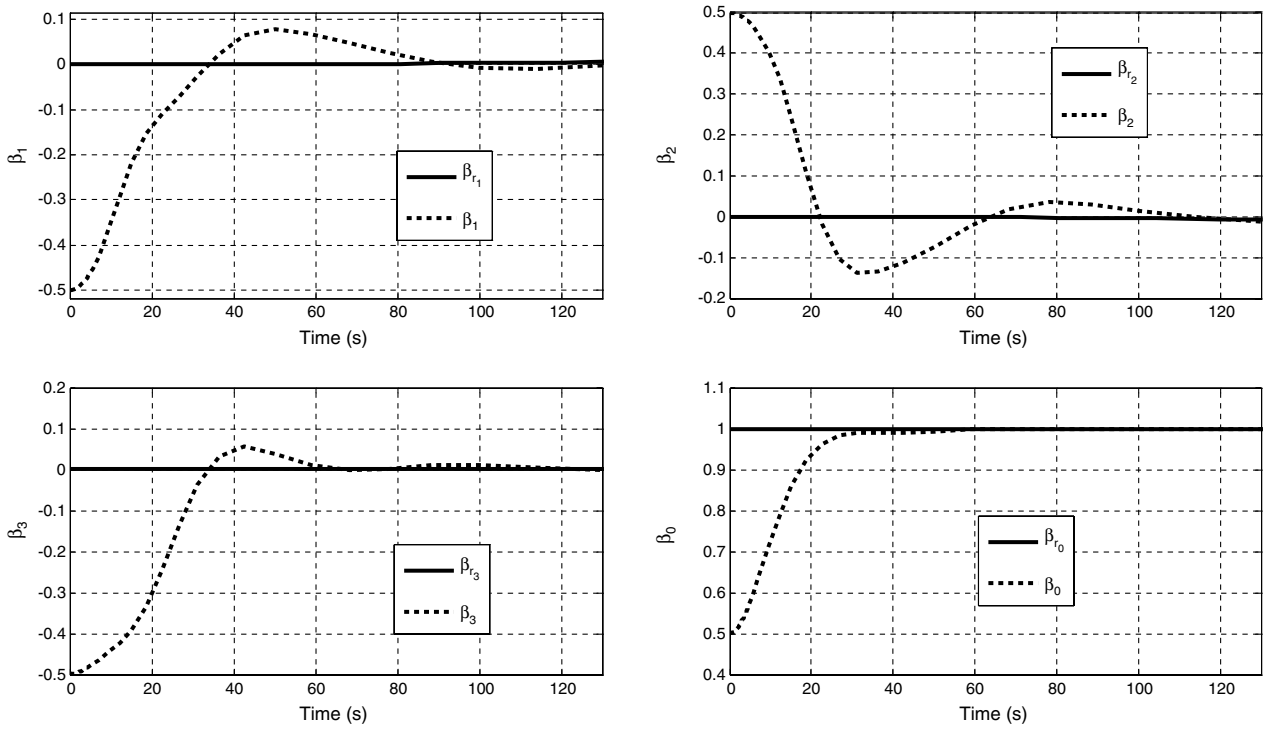

b) Angular position (zoomed)

Fig. 4 More simultaneous steering vehicle results.

$$D\dot{\delta} = \bar{N}_r - F\Omega - E\dot{\Omega} \tag{23}$$

At this point, the shift in thinking changes to the ACS using the EPS inputs (which drive the $E\dot{\Omega}$ term) as a disturbance torque that is accommodated in the steering through this $E\dot{\Omega}$ term. To differentiate VSCMG actuator states that have been measured on the previous time step, a bar is added to the Ω and $\dot{\Omega}$; thus, Eq. (23) becomes

$$D\dot{\delta} = \bar{N}_r - F\bar{\Omega} - E\dot{\Omega} \tag{24}$$

Summarizing the refined steering equations yields

$$\begin{bmatrix} 0_n & D \\ V & 0_n \end{bmatrix} u = \begin{bmatrix} \bar{N}_r - F\bar{\Omega} - E\dot{\Omega} \\ P_c \end{bmatrix} \tag{25}$$

This equation set represents contemporary systems implementing ESACS with flywheel batteries in the electronics loop wherein power is affected by changing $\dot{\Omega}$ and the ensuing attitude disturbance is accommodated in the $E\dot{\Omega}$ term of the gimbal rate steering law. Furthermore, future systems that aim to completely integrate ACS

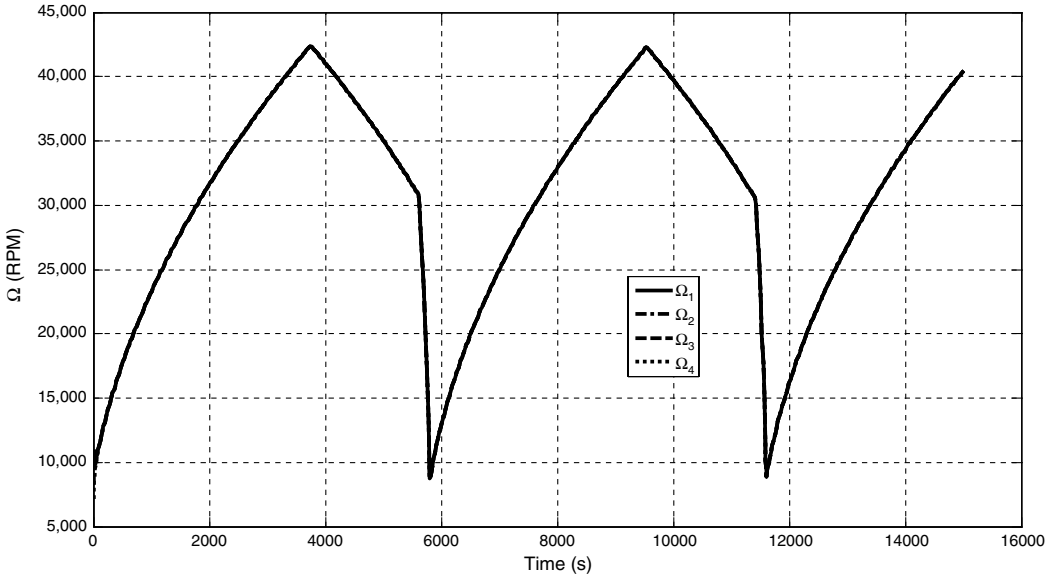

a) Wheel speeds

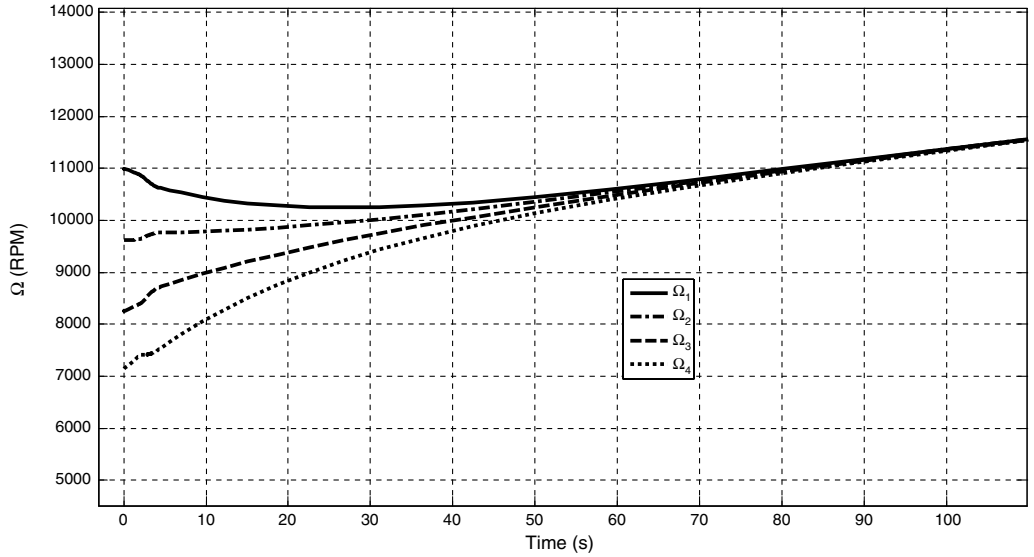

b) Wheel speeds (zoomed)

Fig. 5 Simultaneous steering wheel results.

and EPS by driving $u_c = [\,\dot{\Omega}_c^T \quad \dot{\delta}_c^T\,]^T$ together can use Eq. (25) as an evolutionary stepping stone toward Eq. (17).

The primary limitation of Eq. (25) is that the simultaneous control conducive to VSCMG singularity avoidance through its variable-speed flywheel mode is sacrificed. In addition, the independent control approach is less efficient in its use of the gimbals, as increased gimbal motor power is required to reject wheel disturbance torques while tracking the desired attitude. This concept will be discussed later in the paper. Another limitation of Eq. (25) is that accurate wheel acceleration estimates are required to make this set work. This typically translates directly into estimating the motor current, which is typically directly proportional to the motor acceleration. Although it is far easier to command than it is to measure motor current, even a course estimate can lead to more adequate performance. Examples of the two extremes (i.e., with and without motor acceleration estimates) are presented in Sec. VI and illustrate the impacts this can have on precise satellite pointing. Finally, the existence of accurate wheel speed measurements is assumed; as for most motors, this means measuring/estimating motor voltage (fairly easy to do). Likewise, practical CMGs (which gimbal a fixed-speed rotor) use wheel speed estimates on a regular basis as part of h in the $\omega \times h$, or $F\bar{\Omega}$, term.

VI. Numeric Examples

The following two examples apply the concepts presented previously. The first illustrates the simultaneous steering law for a small satellite system with parameters proportionally similar to the examples found in [30,36–38]. Then the second example uses the same small satellite parameters for two candidate system steering laws (one-way coupled and decoupled).

In these examples, a typical small satellite on a spotlight synthetic aperture radar (SAR) mission in low Earth orbit (LEO) is expected to track a given power profile over more than two orbits, with an orbital period of 5800 s split between a sunlight period (3742 s) and an eclipse period (2058 s). This profile assumes that the subsystems are run at 100% eclipse duty cycle (requiring 100 W instantaneous peak power) with the payload run at 10% eclipse duty cycle (requiring 1000 W of instantaneous peak power). As indicated in Fig. 3a, the first sunlight period runs from 0 to 3742 s followed by eclipse until 5800 s. A conservative assumption made is that the 10% payload duty cycle is requested at the end of each eclipse period (190 s long) when more energy is drained from the wheels than if it occurred at the beginning or even middle of the eclipse. The second orbit thus lasts from 5800 to 11,600 s and also contains

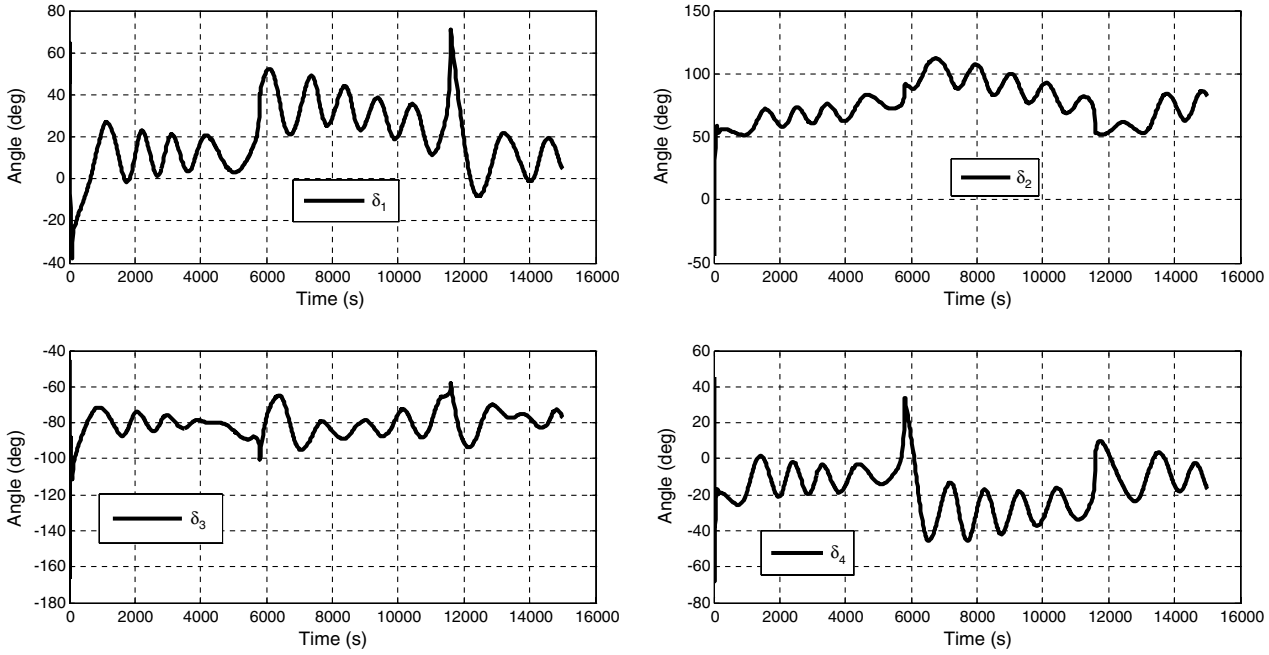

a) Gimbal angles

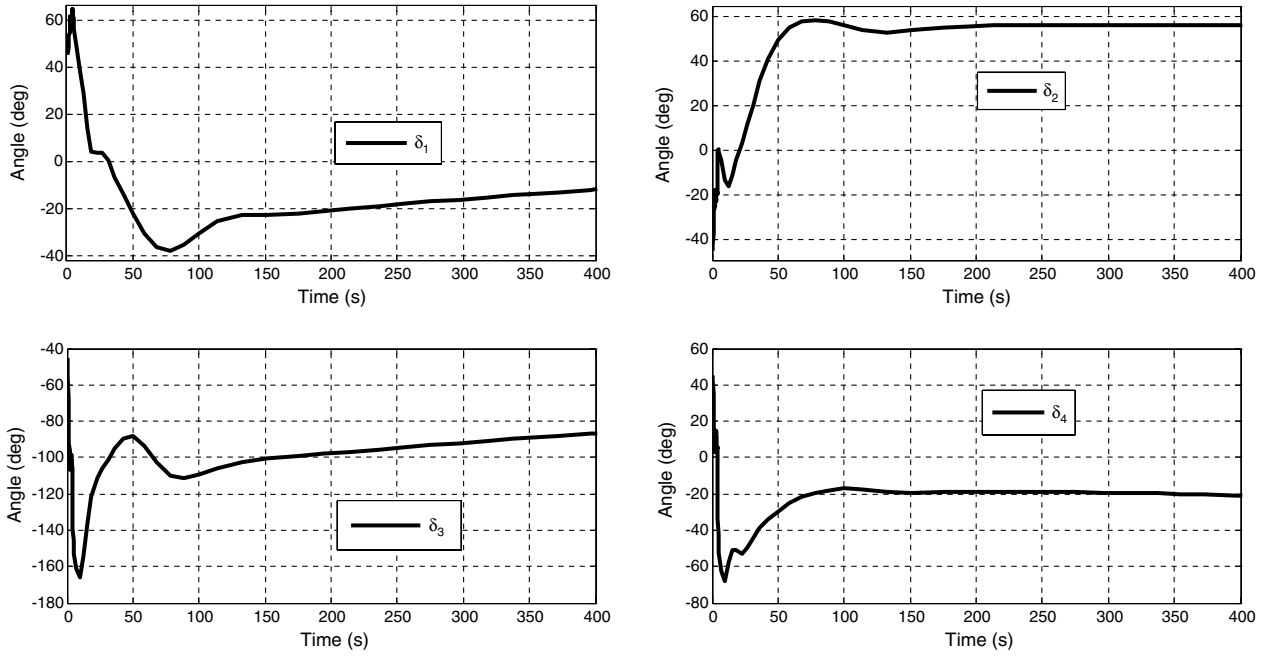

b) Gimbal angles (zoomed)

Fig. 6 Simultaneous steering gimbal results.

a 190 s peak eclipse period in addition to the normal eclipse portion. The satellite is then in sunlight from 11,600 s to the end of the example at 15,000 s.

The attitude profile followed is similar to that given in [37] to aggressively push the controller for agile precision slewing while tracking the desired attitude, as is typical of a spotlight SAR mission. This profile uses three sinusoidal time functions for three-dimensional vehicle slews with respect to the inertial reference frame and spanning the numerical examples' durations. Restated here for clarity, this reference function set is

$$\omega_1(t) = 0.002 \times \sin\left(\frac{2\pi t}{9000}\right) \tag{26}$$

$$\omega_2(t) = -0.003 \times \sin\left(\frac{2\pi t}{12,000}\right) \tag{27}$$

$$\omega_3(t) = 0.001 \times \sin\left(\frac{2\pi t}{10,000}\right) \tag{28}$$

Another important item to mention is that both examples do not treat wheel or gimbal motor friction (for mechanical bearings) or eddy current losses (for magnetic bearings). Such treatment is beyond the scope of the key steering-law objective: implement steering laws for a VSCMG ESACS to advance and validate practical control strategies. In addition, as shown in [33], four primary LEO environmental disturbance torques (solar radiation pressure, gravity-gradient torque, aerodynamic drag, and magnetic torque) were found to be three orders of magnitude smaller than the primary reference torque for these maneuvers. Therefore, the contributions of these disturbance torques are not further investigated.

A summary of the three steering-law cases applied is listed in Table 1. The simultaneous steering example is listed as case 1,

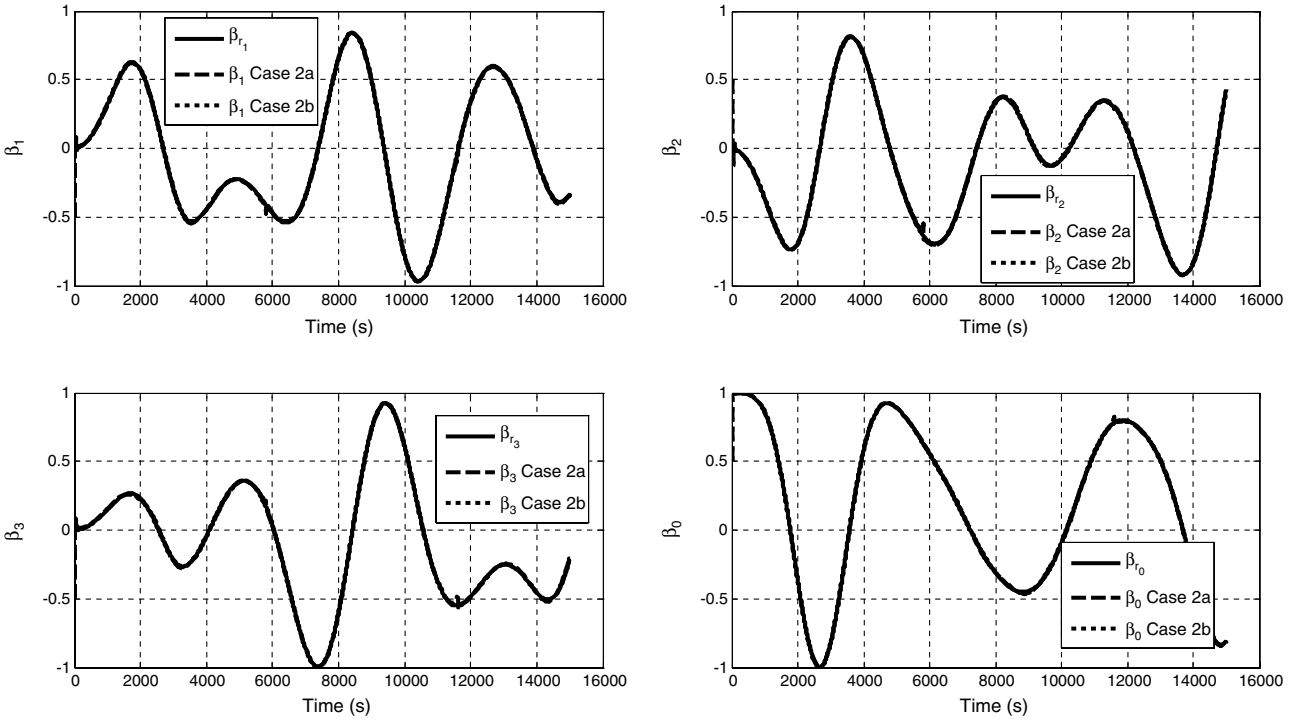

a) Angular position

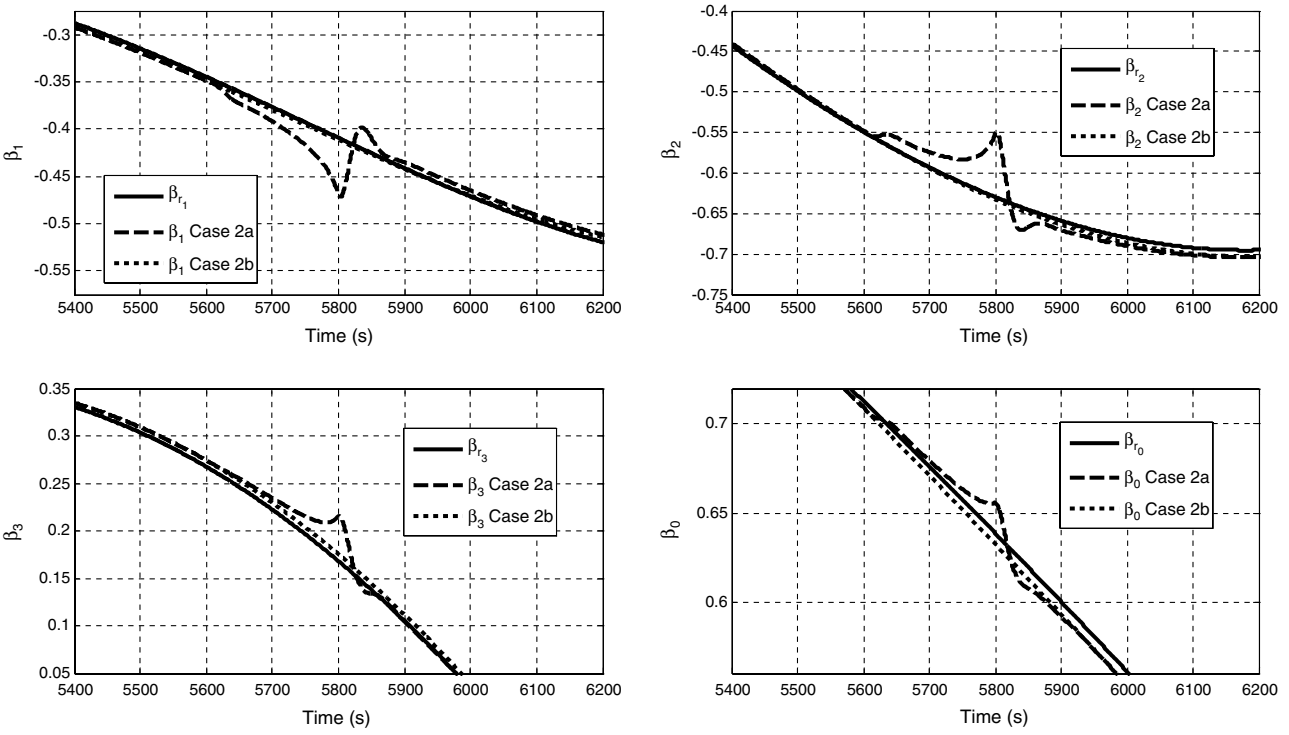

b)Angular position (Zoomed)

Fig. 7 Independent steering vehicle results.

whereas those for the independent steering example are in cases 2a and 2b. Case 1 uses the simultaneous approach applied in [30] along with the VLPID as a vehicle attitude control law. On the other hand, cases 2a and 2b use decoupled and one-way coupled steering laws, respectively, the primary difference being the inclusion of the wheel torque disturbance term $E\dot{\Omega}$, in case 2b. As alluded to earlier, the primary assumption for cases 2a and 2b is that the wheels and gimbals are commanded independently, but the gimbal control will have wheel speed measurements and (for the more practical case 2b) wheel acceleration estimates. Note that several other cases were run using various settings, but these three cases are most representative of the advantages and disadvantages in the steering-law approaches. Parameters for the two examples are given in Table 2.

A. Example 1: Simultaneous Steering Laws

Figures 3a, 3b, 4a, 4b, 5a, 5b, 6a, and 6b illustrate the dynamic responses of the system based on the simultaneous steering law presented, beginning with vehicle power tracking and singularity

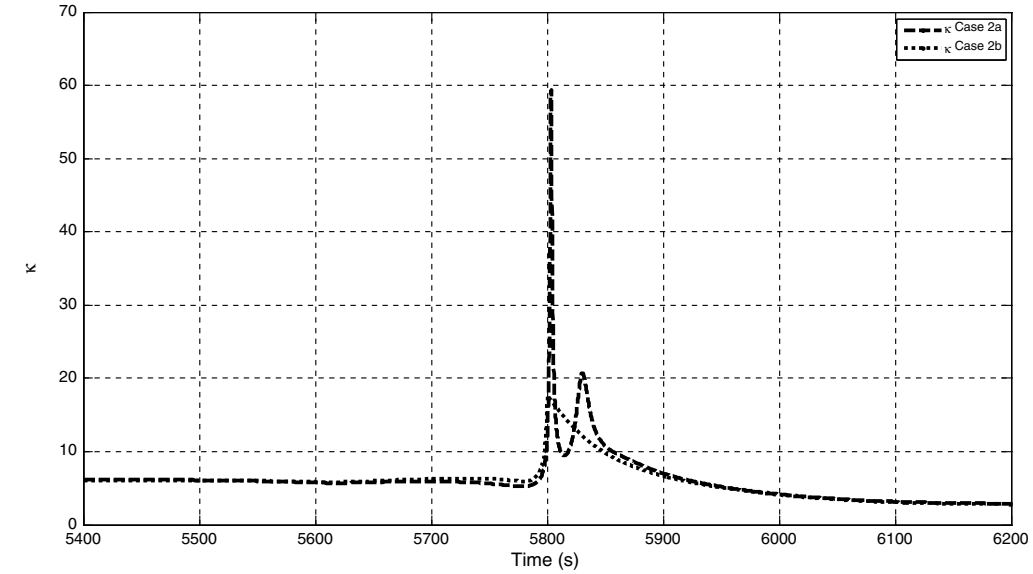

a) Singularity condition

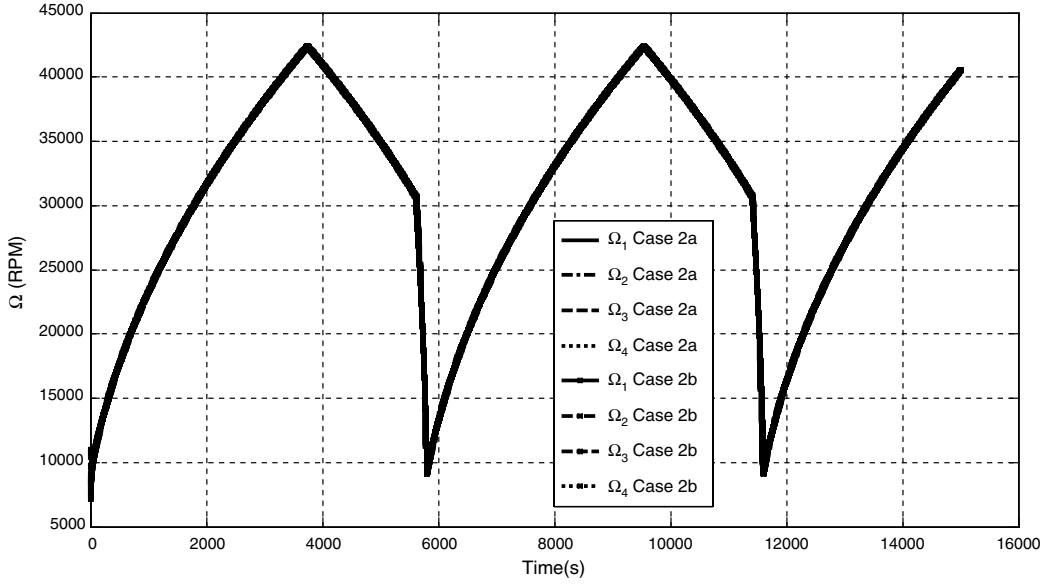

b) Wheel speeds

Fig. 8 More independent steering vehicle results.

index performance, then showing vehicle angular position tracking results, and finishing with actuator (wheel and gimbal) performance responses.

B. Example 2: Independent Steering Laws

Figures 7a, 7b, 8a, 8b, 9a, and 9b, depict the vehicle and actuator performance for two independent (i.e., decoupled and one-way coupled) steering cases (2a and 2b). These results are presented beginning with vehicle angular position tracking, followed by singularity index performance, then finishing with actuator performance responses. As before, the actuators include wheel speed and gimbal angle histories. Analysis of these results and those from the previous example are given in the ensuing section.

VII. Discussion of Results

A. Example 1: Simultaneous Steering Laws

The first example essentially captures the standard attitude plus power tracking case as defined in the literature (albeit with small satellite parameters applied). For this case, the vehicle angular position is reflected in Figs. 4a and 4b. From Fig. 4a, one can tell that each quaternion maintains a relatively close track (in a macroscopic sense) after the first 100–120 s when the desired attitude is acquired, and Fig. 4b amplifies this attitude acquisition phase further. Note that the system is globally asymptotically stable in tracking to the desired attitude. Similar to attitude position, Fig. 3b illustrates that the worst-case singularity condition for case 1 occurs at startup (i.e., the first 100–120 s), when the attitude is acquired. Figure 3a shows the reference power profile and associated track. Here, one can see that power tracking covers more than two orbits (slightly less than three sunlight periods and two eclipse periods). Because uncertainty is not modeled in the vehicle control law, one should note that the actual power tracks the power profile quite closely. Following this power profile very closely, the wheels (as demonstrated in Fig. 5a) have peaks and valleys which match the ends of the charge periods. The acquisition time for the wheels to match the correct power is demonstrated in Fig. 5b. Similarly, the gimbals move quickly during the attitude acquisition phase, as shown in Fig. 6b, then almost periodically over the rest of the scenario (Fig. 6a).

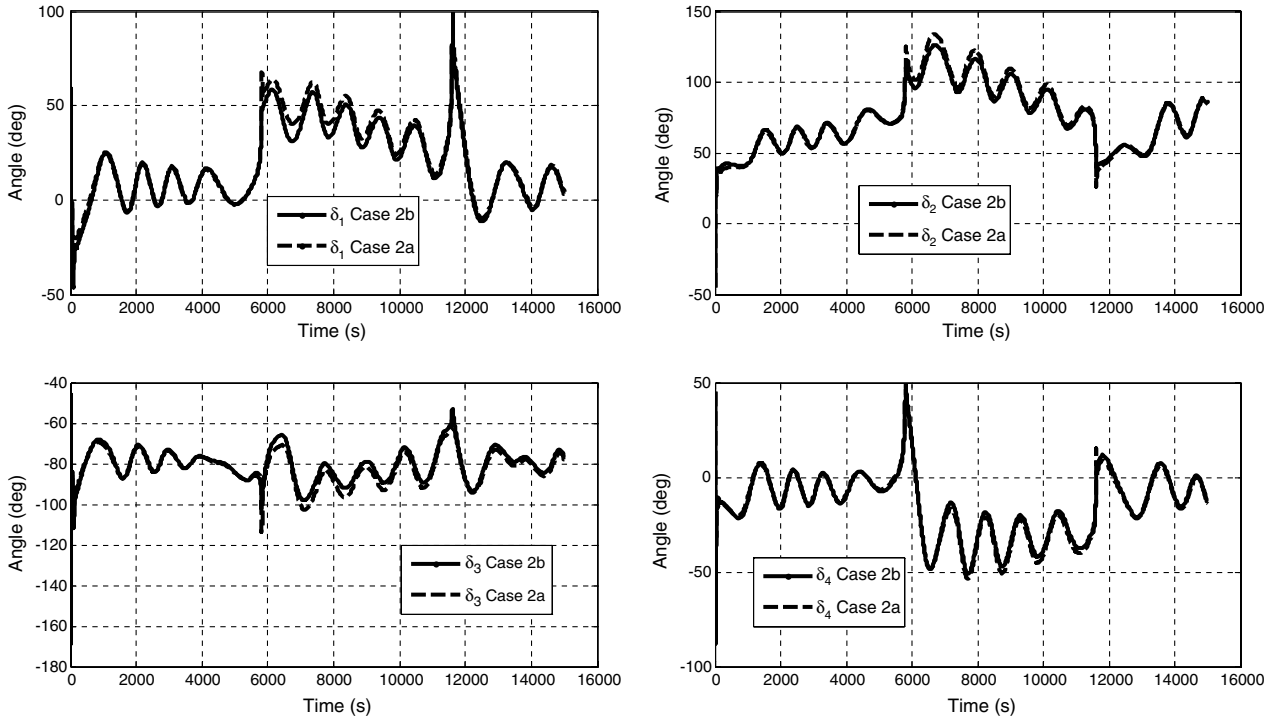

a) Gimbal angles

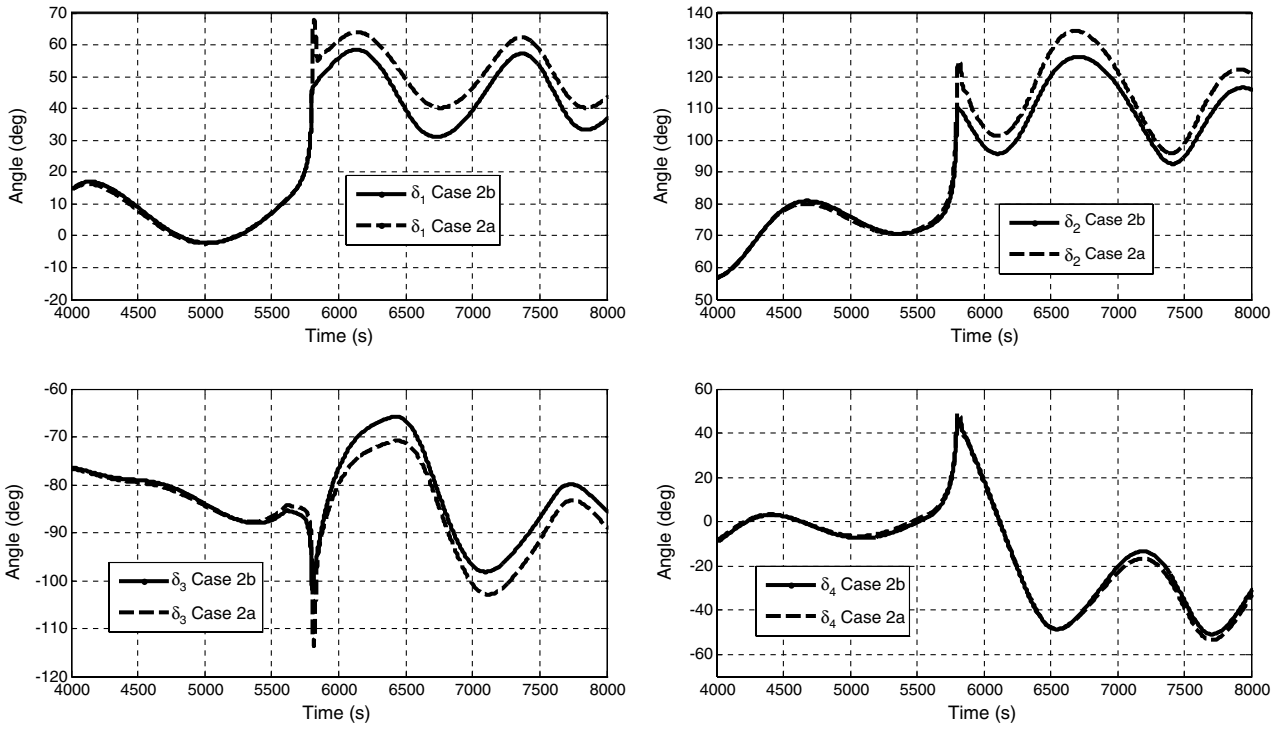

b) Gimbal angles (zoomed)

Fig. 9 Independent steering gimbal results.

B. Example 2: Independent Steering Laws

Next, investigation of the independent steering laws (i.e., decoupled and one-way coupled) yields interesting results as well. These results are captured in Figs. 7a and 7b for the vehicle attitude and Figs. 8a, 8b, 9a, and 9b for the actuator responses that highlight the set 2 cases 2a and 2b. Meanwhile, the power profiles were tracked nearly perfectly in both cases. Because this plot is identical to the power profile for case 1, it has been omitted here for both cases.

First, the vehicles' angular positions are reflected in Figs. 7a and 7b. One may note that the macro view of tracking the attitude for more than two orbits seems fairly benign. However, the view in Fig. 7b pinpoints the performance of these laws during an aggressive part of the maneuver. The choice to further investigate the attitude performance (i.e., zoom-in) of Fig. 7a was selected because the power profile undergoes an ambitious transition over this time period while the vehicle attitude passes through gimbal singularity periods (captured in Fig. 8a). For the power profile, this system transitions from feeding the nominal bus power draw to feeding this bus power plus the SAR payload power draw until the requirements transition from eclipse back to sunlight. Given these two effects, when one

Table 3 Tracking-error comparison

Steering law	Max β_e element	Max P_e, W
1	0.0157	2.2737×10^{-13}
2a	0.1001	4.5475×10^{-13}
2b	0.0171	4.5475×10^{-13}

zooms in on the attitude position plot, this significant error becomes evident. In fact, as one can see, this error lasts more than 100 s. Nevertheless, such position error can be detrimental to a highly sensitive imaging camera or space radar mission in that the wrong ground point may be imaged and power may be temporarily lost to the subsystems until returning to daylight.

In contrast, the associated power plot's power tracking results are very close to the reference for both of the laws and thus they were omitted. This follows from the fact that the power in the one-way coupled implementation only interacts with the wheels. The wheel motion imparts attitude disturbances. This means that the power tracks first by changing the wheel speeds, then the attitude uses this result to react but does not control such wheel response. Thus, both steering laws have very similar power responses with little error.

Next, the singularity index plot shown in Fig. 8a shows a relatively tame singularity condition plot with some growth at the end of the first orbit. Here, one can see that the gimbals stay outside of challenging singularities for most of the maneuver. Correlated to this, the gimbal angle responses shown in Figs. 9a and 9b reflect a fairly benign response: the angles vary similarly to those in the previous example. However, Fig. 9b shows that the gimbal angle histories for cases 2a and 2b split. After initially separating, these gimbal histories have an identical trend due to identical gimbal rate command histories.

Meanwhile, one can see the transitory nature of wheel speeds in Fig. 8b, as the average wheel speed grows to 43,000 rpm and decays back to 9000 rpm at the end of eclipse for each orbit. Note that this figure appears to contain one distinct line as the four wheel speeds for case 2a and the four for case 2b each follow the average speed, which is identical for each case because the power profile is exactly the same. This plot along with the power plots serve to validate the results.

Next, the associated tracking errors for this small satellite maneuver employing the two independent steering laws are captured in Table 3 and Figs. 10a and 10b. From this table and the plots, one can see that the peak-power tracking errors from the independent

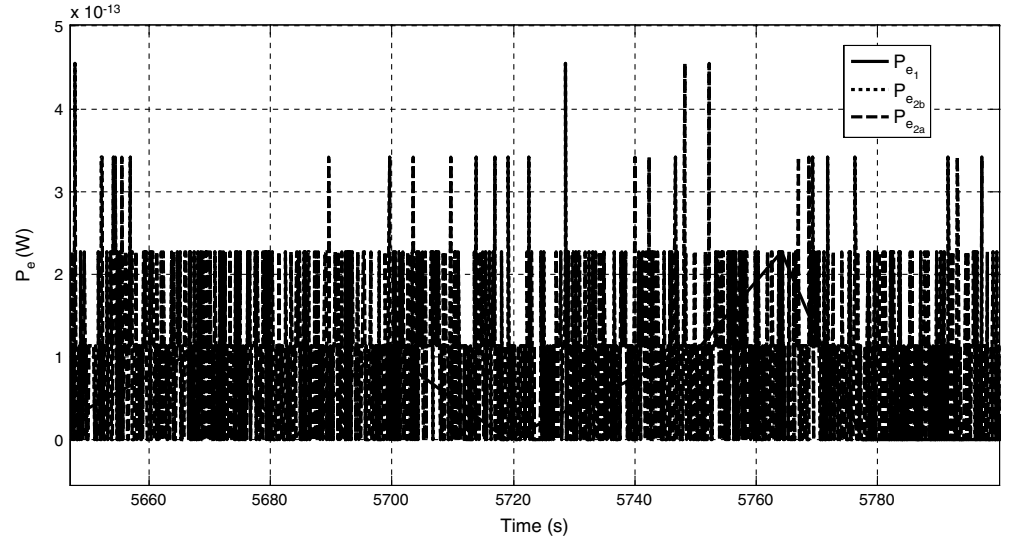

a) Power tracking error

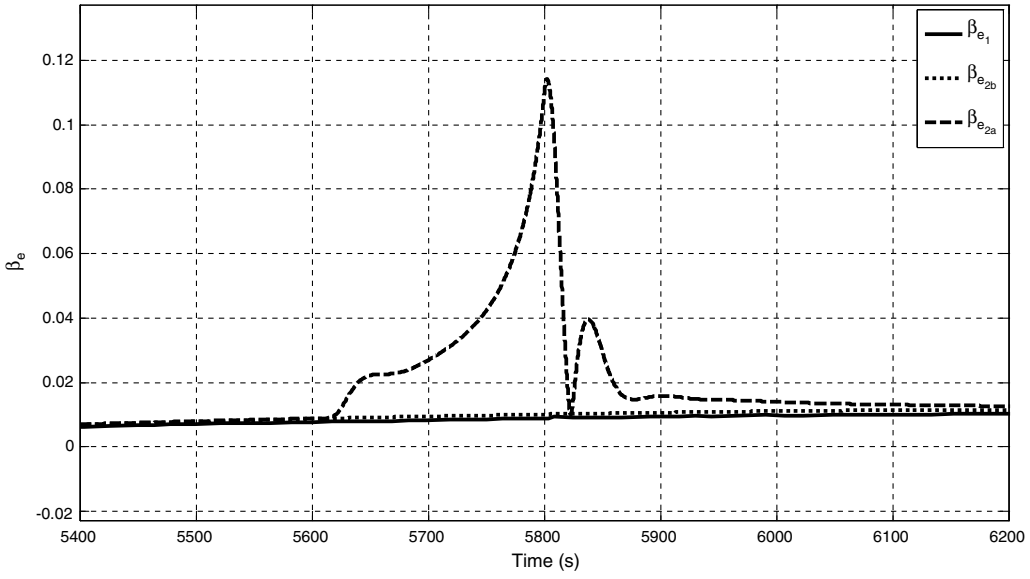

b) Attitude tracking error

Fig. 10 Attitude and power tracking comparisons.

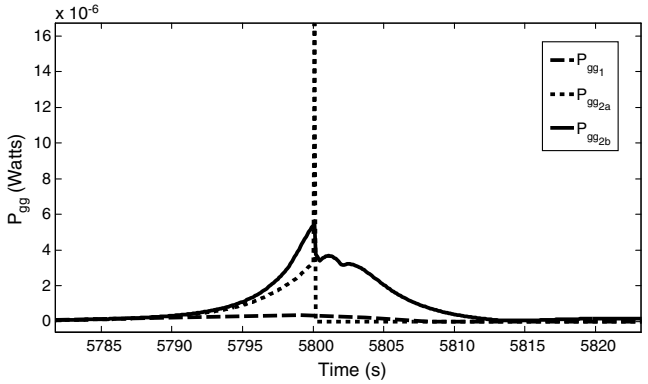

Fig. 11 Gimbal motor power consumption comparison.

case (i.e., one-way and decoupled) are on the same order as the simultaneous steering-law power error, are identical, and are very small. This stems from the fact that the steering laws in the case 2 set only use the wheel speed and acceleration measurement but do not command them. Thus, the true contrast in the laws of cases 2a and 2b arise in the quaternion errors. Here, one can see that the peak quaternion magnitude in case 2a is 5.854 times worse than that of case 2b and 6.376 times worse than that of case 1. Also, as mentioned earlier, the attitude tracking error lasts more than 100 s, during which the case 2a attitude error is well outside of the case 2b error. This stems from the fact that the steering law in case 2b uses information about the wheel acceleration, whereas the case 2a law does not. As shown here, this information is important and should be included in the steering law. For this reason, in the case of independently steering ESACS VSCMGs, steering law 2b, $\dot{\delta}_c = D^{\dagger}(\bar{N}_r - F\bar{\Omega} - E\dot{\Omega})$, is a better suited steering law as compared with steering law 2a. Plus, the additional wheel disturbance torque term $E\dot{\Omega}$ has a significant impact upon the results, especially when peak wheel accelerations are high and wheel spin-axis inertia is low, as in the small satellite example shown here.

Another interesting result found when comparing the two independent control steering laws with simultaneous control is that the separated steering approach, albeit easier to insert into existing energy storage subsystems, consumes more gimbal motor power than in the simultaneous approach. This fact is reflected in Fig. 11, which highlights the difference near the first orbital power drain/storage transition from eclipse to sunlight (i.e., at 5800 s). The gimbal power consumption Pgg is calculated from summing the product of gimbal motor torque N_{gg}, where $N_{gg} = J_{gg}\ddot{\delta}$ and gimbal rate $\dot{\delta}$ for each VSCMG at each time step. Note in this plot that gimbal power for case 2a is much more volatile than for case 2b. In other words, case 2b provides a smoother path during this eclipse-to-sunlight transition. Nevertheless, case 1, the simultaneous steering case, is smoother than both with significantly less magnitude (thus less average power consumption). This points out an important limitation of employing a more immediately practical independent steering algorithm: the gimbals consume more power than in the simultaneous case in order to dampen the wheel disturbance torques generated from separating this control. ESACS control system designers should consider this factor when determining whether or not to implement an independent or a simultaneous steering approach.

VIII. Conclusions

In this work, a novel and simple gimbal steering law was derived to address the practical case when automatic control of the wheels by the electrical power subsystem's electrical circuit topology is conducted independently of the gimbal motors, thus generating the potential for disturbance torques on the spacecraft. These disturbance torques must be accommodated in the attitude steering of the actuators, which is accomplished by the steering law developed. The new law is designed as a linchpin in evolving conventional independent attitude and power subsystems for spacecraft into the simultaneous control contained in the literature. It allows decoupled and practical control of the energy storage and attitude control functions of a combined energy and attitude control system for practical use on small satellites.

Acknowledgments

The authors gratefully acknowledge the project sponsorship from Barrett Flake of the U.S. Air Force European Office of Advanced Research and Development, Brian Wilson of the U.S. Air Force Research Laboratory, and Jerry Fausz of NASA. The authors would also like to thank this paper's reviewers for their very helpful suggestions, especially for the inclusion of the gimbal motor power consumption analysis.

References

[1] Wertz, J. R. (ed.), *Spacecraft Attitude Determination and Control*, D. Reidel, Dordrecht, Holland, The Netherlands, 1978, pp. 201–202.

[2] Hall, C., "Integrated Spacecraft Power and Attitude Control Systems Using Flywheels," Air Force Inst. of Technology, Rept.AFIT/ENY/TR- 000, Dayton, OH, 2000.

[3] Lappas, V., Richie, D., Hall, C., Fausz, J., and Wilson, B., "Survey of Technology Developments in Flywheel Attitude Control and Energy Storage Systems," *Journal of Guidance, Control, and Dynamics*, Vol. 32, No. 2, 2009, pp. 354–365. doi:10.2514/1.32092

[4] Roes, J. B., "An Electro-Mechanical Energy Storage System for Space Application," *Progress in Astronautics and Rocketry*, Vol. 3, 1961, pp. 613–622.

[5] White, J., and Hansen, Q., "Study of a Satellite Attitude Control System Using Integrating Gyros as Torque Sources," NASA TN D-1073, Sept. 1961.

[6] Stickel, H., "Space Qualification Testing of the TELDIX Magnetic Bearing Wheel MWX," *Proceedings of the 1st International Workshop on Spacecraft Attitude and Orbit Control Systems*, ESA, European Space Research and Technology Centre, Noordwijk, The Netherlands, 15–17 Sept. 1997, pp. 221–228.

[7] Eisenhaure, D., Ogleview, R., and Keckler, C., "Energy and Momentum Management of the Space Station Using Magnetically Suspended Composite Rotors," *Proceedings of the 20th Intersociety Energy Conversion Engineering Conference*, Vol. 1, Society of Automotive Engineers, Warrendale, PA, 1985, pp. 197–203.

[8] Rabenhorst, D., "Primary Energy Storage and the Super Flywheel," Rept. TG 1081, Johns Hopkins Univ., Baltimore, MD, Sept. 1969.

[9] Kirk, J. A., "Flywheel Energy Storage Part 1: Basic Concepts," *International Journal of Mechanical Sciences*, Vol. 19, No. 4, 1977, pp. 223–231. doi:10.1016/0020-7403(77)90064-9

[10] Kirk, J. A., and Studer, P., "Flywheel Energy Storage Part 2: Magnetically Suspended Superflywheel," *International Journal of Mechanical Sciences*, Vol. 19, No. 4, 1977, pp. 233–245. doi:10.1016/0020-7403(77)90065-0

[11] Genta, G., *Kinetic Energy Storage: Theory and Practice of Advanced Flywheel Systems*, Butterworths, London, 1985, pp. 1–258.

[12] Danfelt, E., Hewes, S., and Chou, T., "Optimization of Composite Flywheel Design," *International Journal of Mechanical Sciences*, Vol. 19, No. 2, 1977, pp. 69–78. doi:10.1016/0020-7403(77)90001-7

[13] Ratner, J., Chang, J., and Christopher, D., "Composite Flywheel Rotor Technology: A Review," *Composite Materials: Testing and Design*, Vol. 14, ASTM STP 1436, ASTM International, West Conshohocken, PA, 2003.

[14] Bedrossian, N., Paradiso, J., Bergmann, E., and Rowell, D., "Steering Law Design for Redundant Single Gimbal Control Moment Gyroscopes," *Journal of Guidance, Control, and Dynamics*, Vol. 13, No. 6, 1990, pp. 1083–1089. doi:10.2514/3.20582

[15] Jacot, A. D., and Liska, D., "Control Moment Gyros in Attitude Control," *Journal of Spacecraft and Rockets*, Vol. 3, No. 9, 1966, pp. 1313–1320. doi:10.2514/3.28653

[16] Oh, H. S., and Vadali, S. R., "Feedback Control and Steering Laws for Spacecraft Using Single Gimbal Control Moment Gyros," *Journal of the Astronautical Sciences*, Vol. 39, No. 2, April–June 1991, pp. 183–203.

[17] Schaub, H., Vadali, S. R., and Junkins, J. L., "Feedback Control Law for

Variable Speed Control Moment Gyros," *Journal of the Astronautical Sciences*, Vol. 46, No. 3, July–Sept. 1998, pp. 307–328.

[18] Ford, K. A., and Hall, C. D., "Singular Direction Avoidance Steering for Control-Moment Gyros," *Journal of Guidance, Control, and Dynamics*, Vol. 23, No. 4, 2000, pp. 648–656. doi:10.2514/2.4610

[19] Wie, B., Heiberg, C., and Bailey, D., "Singularity Robust Steering Logic for Redundant Single-Gimbal Control Moment Gyros," *Journal of Guidance, Control, and Dynamics*, Vol. 24, No. 5, 2001, pp. 865–872. doi:10.2514/2.4799

[20] Vadali, S., Oh, H., and Walker, S., "Preferred Gimbal Angles for Single Gimbal Control Moment Gyros," *Journal of Guidance, Control, and Dynamics*, Vol. 13, No. 6, 1990, pp. 1090–1095. doi:10.2514/3.20583

[21] Hall, C., "High-Speed Flywheels for Integrated Energy Storage and Attitude Control," *Proceedings of the American Control Conference*, Vol. 3, American Automatic Control Council, Evanston, IL, June 1997, pp. 1894–1898.

[22] Downer, J., Eisenhaure, D., Hockney, R., Johnson, B., and O'Dea, S., "Magnetic Suspension Design Options for Satellite Attitude Control and Energy Storage," *Proceedings of the 20th Intersociety Energy Conversion Engineering Conference*, Vol. 2, Society of Automotive Engineers, Warrendale, PA, 1985, pp. 424–430.

[23] Adams, L., "Application of Isotensoid Flywheels to Spacecraft Energy and Angular Momentum Storage," NASA CR-1971, 1972.

[24] Christopher, D., and Beach, R., "Flywheel Technology Development Program for Aerospace Applications," *IEEE Aerospace and Electronic Systems Magazine*, Vol. 13, No. 6, June 1998, pp. 9–14. doi:10.1109/62.683723

[25] Kascak, P., Dever, T., and Jansen, R., "Magnetic Circuit Model of PM Motor-Generator to Predict Radial Forces," 1st AIAA International Energy Conversion Engineering Conference, AIAA Paper 2003-6068, Aug. 2003.

[26] Roithmayr, C., Karlgaard, C., Kumar, R., Seywald, H., and Bose, D., "Dynamics and Control of Attitude, Power, and Momentum for a Spacecraft Using Flywheels and Control Moment Gyroscopes," NASA TP-2003-212178, April 2003.

[27] Roithmayr, C., Karlgaard, C., Kumar, R., and Bose, D., "Integrated Power and Attitude Control with Spacecraft Flywheels and Control Moment Gyroscopes," *Journal of Guidance, Control, and Dynamics*, Vol. 27, No. 5, 2004, pp. 859–873. doi:10.2514/1.2096

[28] Kenny, B., Jansen, R., Kascak, P., Dever, T., and Santiago, W., "Demonstration of Single Axis Combined Attitude Control and Energy Storage Using Two Flywheels," *Proceedings of the 2004 IEEE Aerospace Conference*, Vol. 4, Inst. of Electrical and Electronics Engineers, Piscataway, NJ, Aug. 2004, pp. 2801–2819; also NASA TM-2004-212935, 2004.

[29] Fausz, J., and Richie, D., "Flywheel Simultaneous Attitude Control and Energy Storage Using VSCMGs," *IEEE International Conference on Control Applications*, Inst. of Electrical and Electronics Engineers, Piscataway, NJ, Sept. 2000, pp. 991–995.

[30] Richie, D., Tsiotras, P., and Fausz, J., "Simultaneous Attitude Control and Energy Storage Using VSCMGs: Theory and Simulation," *Proceedings of the American Control Conference*, American Automatic Control Council, Evanston, IL, 2001, pp. 3973–3979.

[31] Richie, D., Tsiotras, P., and Fausz, J., "Variable Speed Control Moment Gyroscope Workbench: A New Simulation Tool for Tomorrow's Spacecraft," *Proceedings of the 20th Digital Avionics Systems Conference*, Inst. of Electrical and Electronics Engineers, Piscataway, NJ, Oct. 2001, pp. 8A3/1–8A3/12.

[32] Richie, D., Lappas, V., and Palmer, P., "Sizing/Optimization of a Small Satellite Energy Storage and Attitude Control System," *Journal of Spacecraft and Rockets*, Vol. 44, No. 4, 2007, pp. 940–952. doi:10.2514/1.25134

[33] Richie, D., "Combined Attitude Control and Energy Storage for Small Satellites Using Variable Speed Control Moment Gyroscopes," Ph.D. Dissertation, School of Electronics and Physical Sciences, Univ. of Surrey, Guildford, England, U.K., July 2008.

[34] Lappas, V., Steyn, W., and Underwood, C., "Design and Testing of a Control Moment Gyroscope Cluster for Small Satellites," *Journal of Spacecraft and Rockets*, Vol. 42, No. 4, 2005, pp. 729–739. doi:10.2514/1.7308

[35] Varatharajoo, R., "Synergisms for Spacecraft Attitude Control System," Ph.D. Thesis, Technical Univ. of Dresden, Dresden, Germany, printed by Shaker Verlag, Aachen, Germany, June 2003.

[36] Yoon, H., and Tsiotras, P., "Spacecraft Adaptive Attitude and Power Tracking with Variable Speed Control Moment Gyroscopes," *Journal of Guidance, Control, and Dynamics*, Vol. 25, No. 6, 2002, pp. 1081–1090. doi:10.2514/2.4987

[37] Yoon, H., and Tsiotras, P., "Singularity Analysis of Variable Speed Control Moment Gyros," *Journal of Guidance, Control, and Dynamics*, Vol. 27, No. 3, 2004, pp. 374–386. doi:10.2514/1.2946

[38] Richie, D., Lappas, V., and Ashgar, S., "Constrained Singularity Avoidance Using VSCMGs for Combined Attitude and Power Tracking," *Proceedings of the European Control Conference*, Kos Island, Greece, European Union Control Association, Paper WeC10.5, July 2007.

[39] Wie, B., *Space Vehicle Dynamics and Control*, AIAA Education series, AIAA, Reston, VA, 1998, pp. 435–445.

[40] Schaub, H., Vadali, S. R., and Junkins, J. L., "Feedback Control Law for Variable Speed Control Moment Gyros," *Spaceflight Mechanics 1998*, Advances in the Astronautical Sciences, Vol. 99, Univelt, San Diego, CA, pp. 581–600; also American Astronautical Society Paper 98-140, Feb. 1998.

[41] Lappas, V., "A Control Moment Gyro (CMG) Based Attitude Control System (ACS) for Agile Small Satellites," Ph.D. Dissertation, School of Electronics and Physical Sciences, Univ. of Surrey, Guildford, England, U.K., Oct. 2002.

[42] Richie, D., "Simultaneous Attitude Control and Energy Storage Using VSCMGs: Theory and Simulation," M.S. Thesis, Dept. of Aerospace Engineering, Georgia Inst. of Technology, Atlanta, May 2001.

[43] Heiberg, C., Bailey, D., and Wie, B., "Precision Spacecraft Pointing Using Single Gimbal Control Moment Gyroscopes with Disturbance," *Journal of Guidance, Control, and Dynamics*, Vol. 23, No. 1, 2000, pp. 77–85. doi:10.2514/2.4489

[44] Wie, B., Bailey, D., and Heiberg, C., "Rapid Multitarget Acquisition and Pointing Control of Agile Spacecraft," *Journal of Guidance, Control, and Dynamics*, Vol. 25, No. 1, 2002, pp. 96–104. doi:10.2514/2.4854

[45] Lappas, V., and Wie, B., "Robust CMG Steering Logic with Gimbal Angle Constraints," AIAA Astrodynamics Specialist Conference and Exhibit, Keystone, CO, AIAA Paper 2006-6651, Aug. 2006.

[46] Schaub, H., "Novel Coordinates For Nonlinear Multibody Motion with Applications to Spacecraft Dynamics and Control," Ph.D. Dissertation, Texas A&M Univ., Arlington, TX, May 1998.

[47] Larson, W., and Wertz, J., *Space Mission Analysis and Design*, 3rd ed., Kluwer Academic, Boston, 2003, pp. 241–297.